A Motion Direction Map in Macaque V2

Haidong D. Lu,[1,2,*] Gang Chen,[1] Hisashi Tanigawa,[1] and Anna W. Roe[1]
[1]Department of Psychology, Vanderbilt University, Nashville, TN 37240, USA
[2]Present address: Institute of Neuroscience, Chinese Academy of Sciences, 320 Yue-Yang Road, Shanghai 200031, China
*Correspondence: haidong@ion.ac.cn

SUMMARY

In mammals, the perception of motion starts with direction-selective neurons in the visual cortex. Despite numerous studies in monkey primary and second visual cortex (V1 and V2), there has been no evidence of direction maps in these areas. In the present study, we used optical imaging methods to study the organization of motion response in macaque V1 and V2. In contrast to the findings in other mammals (e.g., cats and ferrets), we found no direction maps in macaque V1. Robust direction maps, however, were found in V2 thick/pale stripes and avoided thin stripes. In many cases direction maps were located within thick stripes and exhibited pinwheel or linear organizations. The presence of motion maps in V2 points to a newfound prominence of V2 in motion processing, for contributing to motion perception in the dorsal pathway and/or for motion cue-dependent form perception in the ventral pathway.

INTRODUCTION

Traditionally, area V2 has not been considered a central player in studies of motion processing and direction selectivity. This is not surprising, given the little available data on motion response in V2 and the reports that indicate little directional response in macaque monkey (*Macaca mulatta*) V2 (e.g., Levitt et al., 1994). However, given the well-described anatomical projection from V2 thick stripes to middle temporal area (MT) (Shipp and Zeki, 1985; DeYoe and Van Essen, 1985) and the reportedly higher proportion of directional neurons in the thick stripes (28%) than in the thin (7%) and pale (19%) stripes (Hubel and Livingstone, 1987; Levitt et al., 1994; Shipp and Zeki, 2002; although see Peterhans and von der Heydt, 1993; Gegenfurtner et al., 1996), it was apparent that the role of V2 thick stripes in motion processing deserved further investigation.

We approached this by investigating possible functional organization for direction selectivity in V2. In our view, the presence of a functional organization for a particular parameter points to features that are central to a cortical area's defining role. For example, MT, an area central to motion processing, contains a well-described functional organization for direction selectivity (Albright et al., 1984; Malonek et al., 1994; DeAngelis and

Newsome, 1999). The presence of a hue map in V2 thin stripes reinforces the idea that thin stripes are important for processing of color information (Xiao et al., 2003; Lim et al., 2009). Evidence of functional organization for objects or faces in monkey anterior inferotemporal cortex enhances the concept that it is an area important for object vision (e.g., Wang et al., 1996; Tanaka, 1996). In this vein, we examined whether there are direction maps in V2.

We have established standard methods for revealing the different functional stripe types (thin, pale, and thick) with optical imaging methods (for review, see Roe and T'so, 1997; Roe, 2003; Roe et al., 2007, 2009). As a full thin/pale/thick/pale stripe cycle spans approximately 4 mm, multiple stripes of a single type can be readily imaged within a single cm-sized field of view. Briefly, thin stripes are mapped based on hue-specific responses or by mapping preference to isoluminant color gratings versus luminance gratings of the same spatial frequency (Roe and Ts'o, 1995, 1999; Ts'o et al., 2001; Xiao et al., 2003; Roe et al., 2005; Lu and Roe, 2008; Chen et al., 2008; Lim et al., 2009). Thick and pale stripes can together be identified, although not differentiated, by presence of orientation-selective domains (Ts'o et al., 1990; Roe and Ts'o, 1995, 1999; Ts'o et al., 2001; Ramsden et al., 2001; Roe et al., 2005; Shmuel et al., 2005; Lu and Roe, 2007; Chen et al., 2008). Thick stripes can be distinguished from pale and thin stripes based on preference for binocularity over monocularity (Ts'o et al., 2001) or on the presence of near to far disparity domains (Chen et al., 2008). Some thick stripes contain color-selective cells and color response (Ts'o et al., 2001). Thus, the location of thin, pale, and thick stripes can be determined based on differential imaging methods. In this study, we found clear evidence of direction maps in V2, consistent with locations of thick stripes, and, in contrast, no evidence of direction maps in V1.

RESULTS

Four hemispheres (cases 1–4) in three macaques were imaged in this study. Because the presence of motion maps in V1 and V2 had not been found previously, we wondered whether it could be due to the possibility that motion signals are weak under anesthesia and therefore more difficult to detect. There has also been a report on the presence of more direction-selective neurons in the superficial layers (including layer 2/3) of V1 in awake monkeys than in anesthetized monkeys (Gur et al., 2005). We therefore imaged visual cortex in both anesthetized and awake monkeys (cf. Roe, 2007). Two hemispheres (case 1 and case 3) from monkeys M1 and M2 were imaged in both

Presence of Direction-Selective Domains in V2

Figure 1A illustrates the approximate location of a roughly 2 cm chamber over V1 and V2 and the blood vessel map at this location (Figure 1B). Figures 1C–1G illustrate standard functional organizations revealed in a single imaging session by such large field optical imaging. Each image is a difference map that is obtained by subtracting the sum of images collected from one condition from those of another condition (condition subtractions are illustrated below each image). The V1/V2 border is revealed by imaging for ocular dominance (Figure 1C). Because much of V2 is buried in the lunate sulcus in the macaque, what we know about functional organization in V2 is largely derived from this 1–3 mm region between the lunate and the V1/V2 border (for review, see Roe, 2003). Retinotopic layout of such large fields of view can be imaged by multiple methods (e.g., Lu et al., 2009). We illustrate one method resulting from subtraction of responses to two stationary phase-shifted squarewave gratings (Figure 1D). Typical orientation organization in V1 and V2 can also be imaged, as shown by the color-coded orientation preference map in Figure 1E and the two-orientation subtraction map in Figure 1F. As shown by previous studies (e.g., Roe and Ts'o, 1995; Lu and Roe, 2007; Chen et al., 2008), these orientation maps reveal a pattern of orientation domains in V1 and orientation-selective regions corresponding to thick/pale stripes in V2 (Figure 1F; locations of orientation regions are indicated by cyan bars in expanded views shown in the upper panel of Figure 1J). Color activation maps (subtraction of isoluminant red/green and achromatic luminance conditions) identify locations of blobs in V1 and thin stripes in V2 (Figure 1G; locations of thin stripes are indicated by green arrowheads in the middle panel in Figure 1J) (cf. Roe and Ts'o, 1995; Xiao et al., 2003; Lu and Roe, 2008).

To examine whether there is any functional organization for directional response in V1 and V2, we imaged cortical response to random dot patterns drifting in single directions. Figure 1H shows the direction map obtained by subtracting images obtained in response to two random dot patterns moving in opposite directions (left and right). Since dot size (0.04°), density (10%), speed (8°/s), and luminance (30 cd/m^2) were identical between the two conditions, preference for one condition over the other represents the difference in directional preference (dark pixels: rightward preference, light pixels: leftward preference, shown expanded in Figure 1I). Except for the blood vessels, the map in V1 is largely gray, indicating a lack of detectable direction preference organization in V1. In V2, however, five clusters of dark/white patches are evident (red arrowheads), indicating regions in V2 with preference for rightward (dark pixels) and leftward (light pixels) directional preference. Note that the leftmost red arrowhead in Figure 1I points to a region with two clusters of directional domains (one closer to the lunate sulcus and one closer to the V1/V2 border), indicating that single thick stripes can contain more than one direction-selective region.

Based on correlations previously established (with both electrophysiological and imaging methods) between functional preference (orientation, color, luminance, and disparity) in V2 and CO stripes (thin, thick, and pale stripes) (e.g., Roe and Ts'o, 1995; Ts'o et al., 2001; Moutoussis and Zeki, 2002; Shipp and Zeki, 2002; Xiao et al., 2003; Roe et al., 2005; Lu and Roe, 2008; Chen et al., 2008), we aligned the maps for orientation selectivity, color selectivity, and direction selectivity to determine in which stripes these direction domains are located. As shown in Figure 1J (f, g, and h are enlarged regions of V2 shown in boxed regions of Figures 1F, 1G, and 1H, respectively), the locations of direction-selective domains (indicated by red arrowheads in h) align with the orientation-selective zones (indicated by cyan bars in f) and avoid the thin stripe zones (indicated by green arrowheads in g), indicating that these direction-selective domains fall within thick/pale zones.

In each of the four hemispheres examined, we found direction maps in V2, but no evidence of direction maps in V1. Figure 2 illustrates cortical maps obtained from case 2 (Figures 2A–2C, monkey M2) and case 3 (Figures 2D–2F, monkey M1). In case 2 (Figures 2A–2C), orientation, color, and direction maps were obtained from an anesthetized monkey. Because this is an 8 mm field of view, two stripes of each type are expected within each image. Such imaging reveals alternating regions of orientation preference (Figure 2A, indicated by cyan bars above) that correspond to thick/pale stripes in V2 and regions revealed by color versus luminance preference that correspond to thin stripes in V2 (Figure 2B, indicated by green arrowheads above). The regions of direction selectivity in V2 (Figure 2C, two activation zones indicated by red arrowheads) fall within the locations of thick/pale stripes as revealed by orientation response in V2 (cyan bars from Figure 2A) and fall outside regions preferentially responsive to color (Figure 2B).

Similar Maps in Anesthetized and Awake V2

Figures 2D–2F (case 3) are imaged from an awake, fixating monkey. Plotting conventions are the same as in Figures 2A–2C. Similar to what is seen in the anesthetized monkey, orientation maps reveal broad activation regions in V2 that identify thick/pale stripes (Figure 2D), and color maps reveal largely complementary locations of thin stripes (Figure 2E). In this case, some color activation is observed within the thick/pale region identified by orientation mapping (Figure 2D), consistent with the presence of color response in disparity-selective thick stripes (Ts'o et al., 2001). Directional domains are also observed, located within thick/pale zones in V2 (red arrowheads located in the middle of cyan bars in Figure 2F). The same cortical region in case 3 was also imaged under anesthetized conditions and the same stimulus settings. For cortical regions imaged in both awake and anesthetized conditions (case 1 and case 3), we found that, except for signal magnitude, the anesthetized maps are very similar to the awake ones (See Figure S1 available online).

Relationship of Direction Domains to Thick Stripes

In four hemispheres of three monkeys, we have imaged a total of 12 direction-selective clusters. All of these overlapped with pale/thick/pale stripes of V2 and did not overlap with thin stripes. Nine out of the twelve clusters aligned with the centers of the
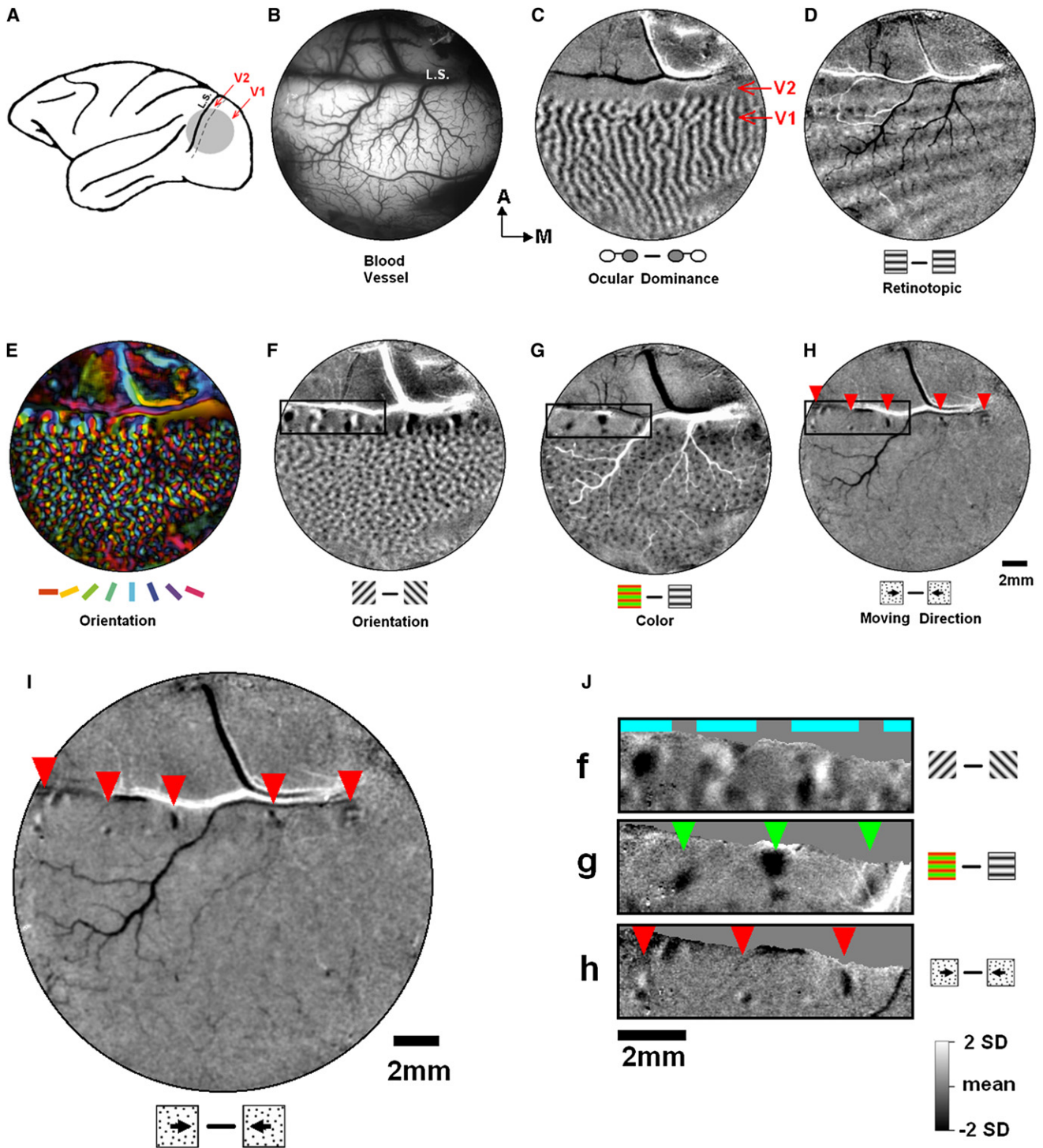
Case #1

Figure 1. Functional Architecture in Macaque Visual Cortex V1 and V2 (Case #1, Monkey M1, Anesthetized)

(A) Illustration of a macaque brain and the approximate location of imaging area. L.S., location of lunate sulcus.

(B) Surface blood vessel pattern of the imaging area.

(C) Ocular dominance map (left-eye minus right-eye stimulation) reveals ocular dominance columns in V1 and lack thereof in V2. The imageable area of V2 is located between the V1/V2 border and the lunate sulcus.

(D) Retinotopic mapping (subtraction of two stationary phase-shifted vertical squarewave gratings) reveals cortical representation of vertical lines in the visual field. Left side of the image is closer to the fovea and has higher cortical magnification.
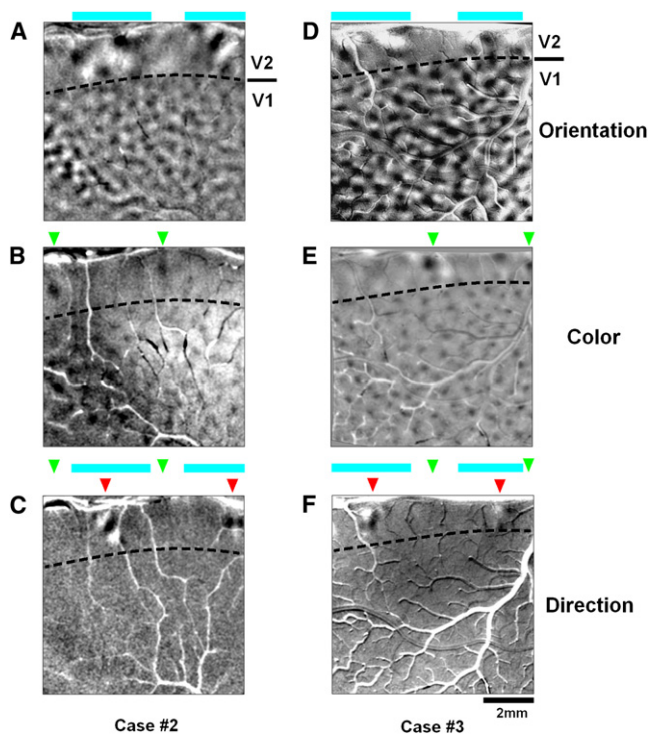
Figure 2. Spatial Relationship between Orientation, Color, and Direction Domains

(A–C) Maps imaged in anesthetized monkey case #2. (A) Orientation map (45° − 135° gratings) reveals typical orientation domains in V1 and thick/pale stripe regions in V2 (cyan bars). Dotted lines on the image indicate the V1/V2 border obtained from ocular dominance maps (not shown). (B) Color map (isoluminant red/green minus luminance gratings) reveals blobs in V1 and thin stripes in V2 (green arrowheads). (C) Direction map (obtained with rightward minus leftward drifting random dot stimuli) reveals direction-selective regions in V2 (red arrows). These domains are located within the thick/pale regions (cyan bars) and avoid the thin stripe regions (green arrowheads). (D–F) Maps obtained from awake monkey case #3 performing visual fixation task. These maps also show that direction domains (indicated by red arrows) are located within the thick/pale regions and avoid the thin stripe regions. Figure conventions are the same as in (A)–(C). Scale bar, 2 mm (applies to all maps). See also Figure S1.

pale/thick/pale stripe regions, consistent with previous reports of direction-selective neurons in V2 thick stripes (Hubel and Livingstone, 1987; Levitt et al., 1994; Shipp and Zeki, 2002).

The remaining three clusters were located within, although not centered on, the pale/thick/pale orientation regions. To further examine the relationship of these direction domains to V2 stripes, we measured the spacing between direction domain clusters. We found that the average distance between two clusters of direction domains in vivo (4.0 ± 0.9 mm, n = 8) is consistent with the spacing between CO thick stripes in histologically processed tissue (4.0–4.25 mm for a full cytochrome oxidase (CO) cycle, Tootell and Hamilton, 1989; Roe and Ts'o, 1995, 1997). Furthermore, direction domains tend to be centered between two thin stripes: the average distance between direction domains and the nearby color domains (thin stripes) is 2.0 ± 0.6 mm, or half of the thin-thin cycle width. The direction clusters were roughly centered between thin stripes, as there was no difference in distance to the medially located (1.9 ± 0.7 mm) and the laterally located (2.0 ± 0.6 mm) thin stripe (t test, p = 0.68). In 11/12 cases, the direction domain clusters were clearly separated from the color activation regions. Only in one case did the direction domains appear adjacent to a color-activated zone. Thus, the bulk of the evidence suggests that the direction domains fall within the thick stripes. Although we do not as yet have histological confirmation of this (as the monkeys are still being used in awake imaging studies), given the amount of functional evidence (mapping for color and orientation), supported with a large body of previous studies, we are confident in our stripe localization. Therefore, our results suggest that direction maps in V2 are localized to the thick/pale stripes and most often correspond to thick stripe locations.

Microarchitecture of Direction Domains

We examined the detailed spatial structure of direction-selective domains within single clusters. Two examples (same domains as the left motion domain in Figure 2C and the left motion domain in Figure 2F) are shown expanded in Figure 3. In Figures 3A and 3C, each of the panels is a subtraction between the direction indicated by the corresponding arrow (shown in the center of figure) and its opposite direction. For example, the right panel in the middle row is a subtraction of rightward (dark pixels: right preferring) and leftward (light pixels: left preferring) drifting random dots. In Figure 3A, comparison of these maps reveals that shifts in stimulus direction results in shifts in the location of activation within the thick/pale stripe. This shifting with respect to direction preference can be viewed in Movie S1 available online. Both difference maps and single-condition maps show shifting of

(E) Orientation vector map. Different colors represent different orientation preferences (color code below; see Experimental Procedures).

(F) Orientation map (45° − 135° gratings) reveals locations of orientation-selective domains corresponding to thick/pale stripe locations in V2 (indicated by cyan bars in top panel of J).

(G) Color map (isoluminant red/green minus luminance gratings) reveals blobs in V1 and color preference domains corresponding to thin stripe locations in V2 (indicated by green arrowheads in middle panel of J).

(H) Motion direction map (rightward minus leftward drifting random dots). Red arrowheads: areas in V2 with directional response preference. No directional preference domains are seen in V1 and other parts of V2. Scale bar in (H) applies to (B)–(H).

(I) Enlarged view of (H).

(J) f, g, and h: Enlarged view of boxed regions of V2 shown in (F), (G), and (H), respectively. Strong blood vessel noise overlying large vessel in lunate sulcus is replaced with even gray (top portion of each panel). Thick/pale stripes (indicated by cyan bars) contain orientation preference domains (f). Thin stripes (indicated by green arrowheads) contain color preference domains (g). Note that color preference regions (green arrowheads in g) occur in regions with poor orientation selectivity (even gray zones aligned with spaces between cyan bars in f) and interdigitate with orientation-selective regions. Directional domains (h, red arrowheads) fall within thick/pale stripe zones and avoid thin stripe zones.

Maps (C)–(J) are displayed using the gray scale shown in the lower-right corner (SD: standard deviation of pixel distributions for each individual maps).
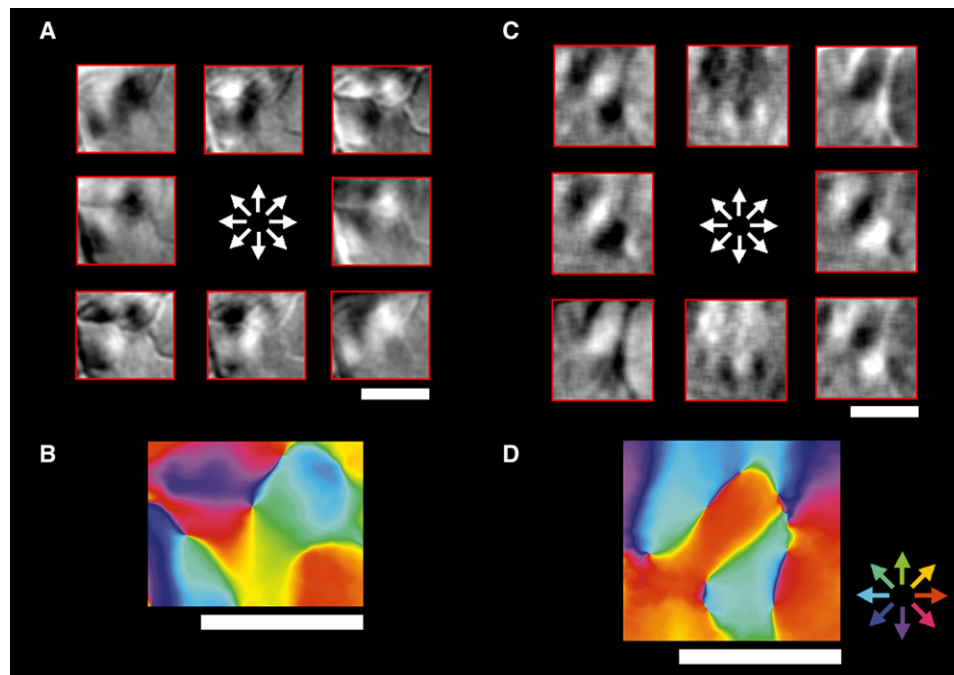
Figure 3. Zoomed-in Views of the Direction Domains

(A) and (B) are from case #3 awake (top left arrowhead in Figure 2F). Each panel in (A) is the difference between the direction indicated by the corresponding arrow and its opposite direction. Note that location of activation zone within the thick/pale stripe shifts as stimulus direction shifts. (B) is a vectorized summation of the eight panels in (A) and each direction is coded in a specific color (color index at the lower right corner). It reveals a pinwheel-like pattern. Also see Movie S1, which reveals that activated regions shift smoothly with each shift in the direction of the moving random dots, resulting in a pinwheel-like pattern. (C) and (D) are from case #2 anesthetized (top left arrowhead in Figure 2C). Plotting conventions are the same as in (A) and (B). Unlike the direction domains shown in (A) and (B), the direction domains in this case do not form a pinwheel pattern. Instead, regions preferring different directions shift linearly (do not rotate). Scale bars in (A)–(D): 1 mm. See also Figure S2 for single-condition maps.

focal activation in response to random dot patterns drifting in different directions (see Figure S2).

The movie reveals that activated regions shift smoothly with each shift in the direction of the moving random dots, resulting in a pinwheel-like pattern. This systematic representation is also illustrated in Figure 3B, which is the vectorized summation of these eight panels in Figure 3A. Thus, within this approximately mm-sized region, all directions tested are represented, suggesting the presence of a complete directional map within each direction cluster. In addition to pinwheel-like organizations, we also observed linear type organizations. In the case shown in Figures 3C and 3D, regions selective for leftward direction preference alternated with those for rightward direction, suggesting a more linear mapping organization. Roughly half of the motion regions exhibited pinwheel-like organization, while others were more linear in organization. Thus, not unlike orientation domains in V2, both pinwheel and linear organizations are observed.

Relationship with Orientation Preference

Previous studies have shown that the preferred direction is usually orthogonal to the preferred orientation, and thus the direction map is strongly correlated with the orientation map (Malonek et al., 1994; Weliky et al., 1996; Shmuel and Grinvald, 1996). To examine the relationship between the direction and orientation maps, for each case we calculated vector maps for

both direction and orientation selectivity. Figure 4 illustrates the comparison of vector maps for direction selectivity and orientation selectivity (case 3, same cortical area as in Figure 2F). In the direction vector map shown in Figure 4A, the hue represents the preferred direction and the saturation represents the strength of selectivity. The two regions of directional selectivity in V2 are clearly distinguished (red arrows above Figure 4A indicate two regions of saturated color in V2). The direction region shown in Figure 4A (in the white frame) is shown enlarged in Figure 4B. The direction (arrows) and orientation preferences (bars) at each location are overlaid on the vector map.

The relationship of this direction map was then directly compared with the orientation map. As shown in Figure 4C, the orientation vector map of the same cortical region (obtained using sinusoidal gratings presented at four different orientations) reveals clear orientation maps in V1 and in V2 thick/pale stripe regions. The same region enlarged in Figure 4B (in the white frame) is shown enlarged in Figure 4D. As shown by overlaying the direction (arrows) and orientation preferences (bars), it appears that the preferred orientations tend to be orthogonal to the preferred direction. This impression is quantified in Figure 4E, which plots the distribution of the difference between these two angles (preferred direction and preferred orientation). This distribution illustrates a strong bias toward orthogonality and is significantly different from uniform (χ^2 test, $p < 0.001$). In
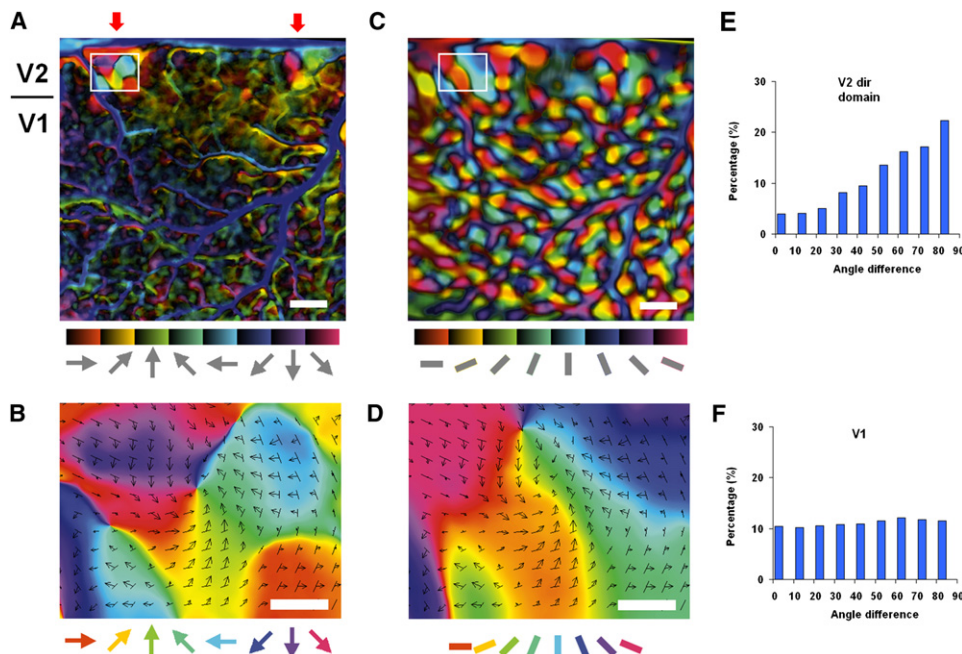
Figure 4. Angles of Preferred Direction and Preferred Orientation in V1 and V2

(A) Vector summed response to eight different directions. Colors indicate preference for different directions (color index below). Saturation indicates the strength of the direction selectivity (the length of the vector).

(B) Enlarged angle map of the framed region in (A). Arrows: preferred direction at each location. Short bars: preferred orientation. The lengths of the arrows/bars are proportional to the strength of the direction/orientation selectivity.

(C) The orientation vector map of the same field of view as in (A).

(D) Enlarged angle map of the framed region in (C). Arrows and bars represent preferred direction and orientation (same as in B).

(E and F) Distribution of the angle differences between preferred direction and preferred orientation in direction domains in V2 (E) and the whole V1 region (F). The relationship tends to be orthogonal in V2, but not in V1.

Scale bars: (A) and (C), 1 mm; (B) and (D), 250 μm.

contrast, in V1 (Figure 4F), the distribution of relative orientation and direction differences is flat (χ^2 test, p > 0.9). Thus, this analysis supports the presence of a predominantly orthogonal relationship between orientation and direction within the V2 direction domains, a relationship that is consistent with previous electrophysiological studies (Hubel and Wiesel, 1962; Albright et al., 1984) and optical imaging studies (Malonek et al., 1994; Weliky et al., 1996; Shmuel and Grinvald, 1996). Notably, there is a lack of a systematic relationship between orientation and direction in V1, which provides further support for the lack of directional domains in V1.

Apparent Lack of Directional Maps in V1
The possibility remains that our imaging methods are unable to detect motion response in V1, due to either weakness of response or to the possibility that motion-selective neurons reside in relatively deep cortical layers (layer 4B and 6), at depths beyond the reach of our optical measurements. We cannot eliminate the possibility that there are direction maps in deeper layers. However, to test whether our imaging methods are capable of detecting the presence of motion response in V1, we asked whether we could detect "axis-of-motion" maps. To test this, we used drifting random dot fields with slow speeds (1°/s, sufficiently slow that the moving dots would not induce

motion streak phenomena where very fast moving dots produce the percept of an oriented line; see Geisler, 1999; Geisler et al., 2001). By subtracting two sets of orthogonal moving stimuli (i.e., sum of up and down directions minus sum of left and right directions), we observed an axis-of-motion map (Figure 5A), demonstrating that motion signal alone could produce structured maps in V1. This indicates that the optical imaging method is capable of detecting motion signal.

Detailed examination revealed that such an axis-of-motion map is very similar to an orientation map generated by subtracting two sets of orthogonal sinewave gratings (Figure 5B, compare insets in Figures 5A and B5). Response profiles (cf. Basole et al., 2003) of these two maps (Figures 5A and 5B right column) also indicate that the peak response pixels of these two maps are located at the same regions (i.e., white pixels fall in 90° orientation domains). This means that pixels activated by horizontal gratings were also activated by vertical moving random dots, while pixels activated by vertical gratings were also activated by horizontal moving random dots. This is exactly what is expected when direction cells are imaged since direction selectivity and orientation selectivity tend to be orthogonal to each other. In contrast, subtracting random dot patterns moving in two opposite directions results in a subtraction of two similar signals and a flat map (Figures 5C and 5D).
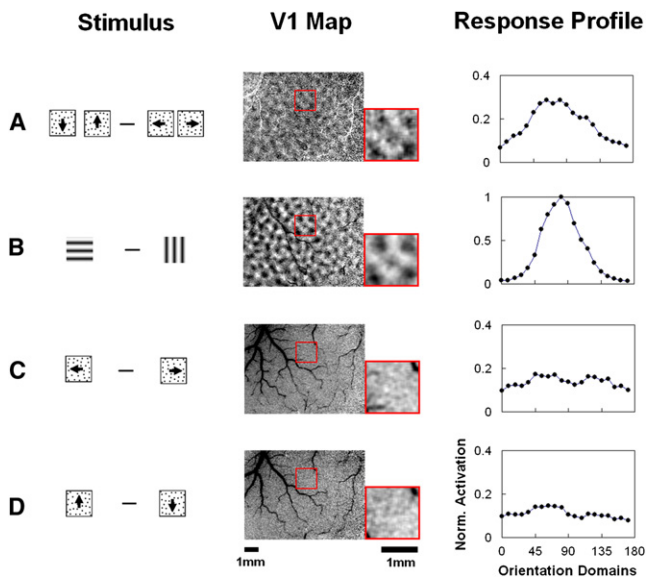
Figure 5. Motion Signals in V1 Are Detectable by Optical Imaging
(A) Vertical versus horizontal axis-of-motion map: the subtraction of two orthogonal moving axes (sum of up and down minus sum of left and right fields of drifting random dots, speed 1°/s). Subtraction of two moving axes reveals weak but regular patterns. Detailed comparison (region in red box expanded at right) indicates that this map is similar to the orientation map shown in (B). The response profile (right column) of the entire field of view (all V1) also indicates such similarity. This map suggests that the vertical-moving random dots activate the same domains that are activated by horizontal gratings, and horizontal moving random dots activate the same domains activated by vertical gratings. This is consistent with the orthogonal relationship between orientation and direction selectivities. (B) Horizontal versus vertical orientation map obtained with sinewave gratings. Response profile on the right indicates the positive activation is located in vertical domains (90° angle). (C) Subtraction maps obtained with horizontal drifting random dot patterns (left minus right). Although this figure uses the same data that are used in (A), the map is basically flat. The flat response profile also indicates that there is no apparent correlation between this map and orientation map. A similar finding is true for (D), which is a subtraction of two vertical moving random dot patterns (up minus down). Scale bars (1 mm) are shown under corresponding original and magnified maps.

Our point here is that the lack of direction maps in V1 is not due to an inability to image motion response in V1. The fact that we observe axis-of-motion maps (Figure 5A) indicates that our imaging methods do indeed detect motion response in V1, but that this motion response is not organized in a directionally specific manner. This does not exclude the possibility that direction segregation may still exist at deeper layers (e.g., layer 6) beyond the scope of imaging methods used here or that the direction domains are too small to resolve with these methods (see Discussion).

DISCUSSION

Summary

The present study is the first demonstration of a map for direction selectivity in macaque V2. These direction-selective domains are observed in maps that contrast two opposite directions.

Standing random dots or random dots undergoing random motion (wiggly dots) do not result in such maps (data not shown). Furthermore, these direction-selective domains exist only in specific locations in V2: within the orientation-selective zones or thick/pale stripes of V2. In a majority of cases, these domains fell within the center of the thick/pale extent, consistent with thick stripe locations. Similar to direction maps in other areas and other species, the preferred directions tend to be orthogonal to the preferred orientations (Hubel and Wiesel, 1968; Albright et al. 1984). Direction maps were not observed in V1 with these optical imaging methods.

Direction Maps in V2

In the present study, direction maps in V2 were observed in each case examined (n = 4). The spatial patterns of these domains are independent of the following factors: (1) awake versus anesthetized condition, (2) stimulus type (random dots or sinusoidal gratings), and (3) time (over a year of repeated awake imaging). These all suggest that direction maps are an intrinsic feature of V2, similar to other functional maps (e.g., orientation, color, and disparity maps), and are not an artifact of anesthesia or stimulus type.

We find that direction maps in macaque V2 are located within the thick/pale regions of V2. Although monkeys imaged in this study are still being used in awake imaging studies and thus the CO histology is yet not available, based on the well-established correlation between stripe type and functional response (Hubel and Livingstone, 1987; Roe and Ts'o, 1995; Ts'o et al., 2001; Moutoussis and Zeki, 2002; Shipp and Zeki, 2002; Xiao et al., 2003; Lu and Roe, 2008; Chen et al., 2008), we are confident about the stripe location of direction domains. Several arguments suggest that these directional responses are concentrated within the thick stripes of V2. Imaged directional domains are located within orientation regions of V2 (thick/pale stripes) and never within color-preferring regions (thin stripes). These direction-selective domains are frequently (9 out of 12) centered within the orientation-selective regions in V2, consistent with thick stripe location. Our measurement of the average distance between two direction domains (4.0 ± 0.9 mm) suggests that direction domains share a periodicity similar to the thick stripe periodicity. Moreover, while orientation domains and color domains are seen to abut, there are gaps between direction domains and color domains. Thus, the bulk of the evidence suggests that the direction domains fall within the thick stripes.

Previous studies are consistent with these findings. Anatomically, thick stripes in V2 are the main recipient of direct input from V1 layer 4B (Livingstone and Hubel, 1987), a layer that is rich in direction-selective cells. Thick stripes are also the only source of anatomical projections from V2 to MT (DeYoe and Van Essen, 1985; Shipp and Zeki, 1985), an area marked by motion-selective responses and functional organization for motion response (Albright et al. 1984; Malonek et al., 1994; DeAngelis and Newsome, 1999; Xu et al., 2004). Tootell and Hamilton (1989) reported in their 2-deoxyglucose study possible clustering of directional response in V2. Using a random dot field moving in a single direction, they revealed a mottled stripe-like appearance in V2, but provided no correlation of these patterns with stripe locations. Electrophysiological studies

(e.g., Levitt et al., 1994; Shipp and Zeki 2002) indicate a greater presence of direction selectivity in thick stripes than in other stripe types. Consistent with thick stripe function (cf. Schmolesky et al., 1998; Schroeder et al., 1998), directionally selective cells have the shortest latencies in V2: median 66 versus 69–85 ms (Munk et al., 1995, Table 3). Thus the localization of these direction domains to thick stripes is consistent with a body of evidence pointing to the role of thick stripes in directional response.

We note that the organization of directional domains in V2 is not spatially congruent with that of orientation domains in V2, as they occupy only portions of the full orientation map extent in V2 thick/pale stripes. We suggest therefore that these directional maps are not simply a by-product of orientation response in V2, but are an organization in their own right. How does such organization arise? We speculate that the presence of direction domains in V2 thick stripes results from selective integration of motion inputs from V1. The fact that a clustering of directional selectivity arises only in secondary motion processing areas such as V2 and MT, and not at the first stage of motion processing (V1), suggests that creation of such clustering involves a two-stage process. In addition, there may be some as yet undetermined relationship between motion maps (this paper) and disparity maps (Chen et al., 2008) in the thick stripes of V2. The fact that motion maps, disparity maps, and hue maps arise in secondary areas (V2 and MT), but not the first stage (V1), may indicate common functional transformations across feature modalities (cf. Roe et al., 2009).

We also note that localization of direction-selective response to thick stripes may be the reason that fMRI studies find relatively low (0.35 in V2 compared with 0.84 in MT; Tolias et al., 2001) or complete lack of direction-selective response in V2 (Smith and Wall, 2008; note distinction between direction-selective response and motion response; cf. Vanduffel et al., 2001). Because the BOLD signal detected in fMRI typically does not have the resolution to reveal stripe-specific activation, any direction-selective BOLD activation observed in V2 may be diluted by non-direction-selective response outside of thick stripes.

Lack of Direction Maps in V1?
In early visual cortical areas of the carnivore, direction maps are readily observed (area 17 of the ferret: Weliky et al., 1996; area 18 of the cat: Shmuel and Grinvald 1996; Ohki et al., 2005). Electrophysiological studies in the cat reveal columnar organization of cells with similar direction selectivity (Payne et al., 1981; Swindale et al., 1987). Consistent with electrophysiology, optical imaging of cat and ferret visual cortex show that orientation domains are divided into direction-preference domains with direction preference orthogonal to orientation preference (Weliky et al., 1996; Shmuel and Grinvald, 1996; Ohki et al., 2005). Direction maps are also present in area MT of old world monkeys (macaque: Albright et al., 1984; DeAngelis and Newsome, 1999; Cebus: Diogo et al., 2003), new world monkeys (owl monkey: Malonek et al., 1994; Born, 2000; Kaskan et al., 2010), and galagos (Xu et al., 2004).

However, thus far, despite the many studies that have been conducted, there has been no electrophysiological evidence for columnar organization of directional selectivity in either in V1 or V2 of the macaque (Hubel and Wiesel, 1968; Dow, 1974;

De Valois et al., 1982; Livingstone and Hubel, 1984). Accordingly, electrophysiological studies in monkey V1 reveal frequent reversals of direction selectivity within vertical penetrations (Hubel and Wiesel, 1968), consistent with a lack of directional maps in V1.

Although we did not find evidence for directional maps in V1, it remains possible that direction cells in macaque V1 are located at a depth beyond the purview of these optical imaging methods. The directionally selective cells found in macaque V1 (roughly one-fourth to one-third of the population) are concentrated in deeper layers in layers 4B, mid-4C, and 6 (Schiller et al., 1976; Gilbert, 1977; De Valois et al., 1982; Livingstone and Hubel, 1984; Orban et al., 1986; Hawken et al., 1988; Gur et al., 2005). V1 neurons projecting to MT are almost exclusively direction-selective neurons from either layer 4B or the boundary of layers 5 and 6 (Movshon and Newsome, 1996). Interestingly, layer 4B neurons projecting to MT are mainly spiny stellate neurons, whereas those layer 4B neurons projecting to V2 are mainly pyramidal neurons (Nassi and Callaway, 2007).

What our data suggest is that, if there are directional domains in V1, they are unlikely to lie in the superficial layers of V1. The fact that we were able to image axis-of-motion maps (Figure 5) indicates that our imaging methods are capable of detecting coherent motion signal from V1 (whether they are derived from direction-selective cells and/or orientation-selective cells). Note that the axis-of-motion map is not a result of the motion streak effect (Geisler, 1999; Geisler et al., 2001; Mante and Carandini, 2005) since (1) the motion streak effect occurs only at relatively high speeds (>4°/s for the dot size we used) and (2) the motion streak map is not orthogonal to the orientation map (i.e., at high speeds horizontal moving random dots would activate horizontal orientation domains).

We would also argue that our inability to see direction domains in V1 is unlikely to be due to insufficient spatial resolution. As orientation domains in other areas (e.g., in cat area 17 and 18) comprise two direction domains of opposite direction preference, one would expect direction domains to be roughly half the size of orientation domains. If direction-selective domains do exist in macaque V1, a reasonable estimate of their size should be 0.1–0.25 mm (i.e., half of the orientation domain size). Functional domains of such a size, such as color blobs in V1, are readily detected by optical imaging methods. We routinely detect color blobs (which are 0.15–0.2 mm in size) in V1 (Lu and Roe, 2008) and even subregions of single blobs that exhibit different hue preference (Xiao et al., 2007; Roe et al., 2009). Although one still cannot rule out the possibility that the size of directional clustering is so small (e.g., <0.05 mm) that it is beyond the resolution of the intrinsic optical imaging method, the evidence so far (both electrophysiological and imaging) does not support the presence of such an organization.

Given our results, we would like to suggest that motion response is organized in the superficial layers of V1 (i.e., according to their preferred motion axis), but neurons preferring opposite directions in these layers are not spatially segregated (Figure 6, left). This is in contrast to neurons in V2, which are segregated with respect to both orientation and direction preference (Figure 6, right).
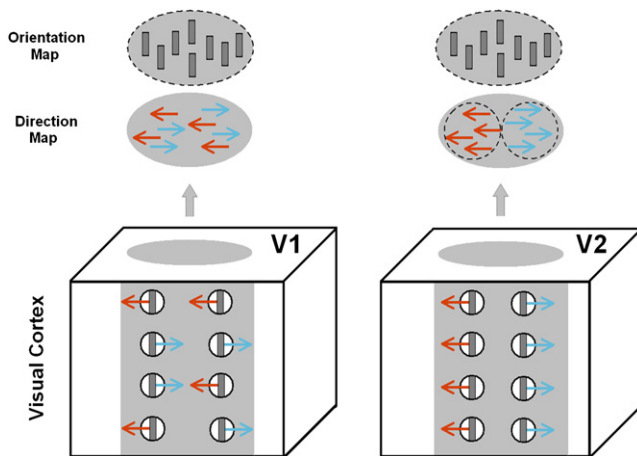
Figure 6. One Depiction of Why Direction Maps Are Observed in V2, but Not in V1

The two cubes represent the gray matter of V1 and V2. The small circles represent neurons with preferred orientation (short gray bars in the circles) and preferred direction (red and blue arrows). In V1, although neurons are organized according to their preferred orientation, neurons preferring opposite directions are spatially mixed. Such organization results an orientation map and an axis-of-motion map but no direction map (top ovals). In V2, both orientation maps and direction maps are observed because neurons preferring opposite directions are further segregated. Dashed circles within the ovals indicate clustering of orientation or direction signals, leading to observed orientation and direction maps.

Possible Role of V2 Motion Signals in the Dorsal Pathway

Given that thick stripes project anatomically to area MT, what functional contribution does this input provide to MT? In a study that directly addressed the functional contribution of V2 to MT via inactivation of V2 and V3, it was reported that such inactivation led to loss of disparity-selective, but little direction-selective, response in MT (Ponce et al., 2008). Consistent with the strong presence of disparity response in the thick stripes of V2 (Hubel and Livingstone, 1987; Ts'o et al., 2001; Chen et al., 2008) and in V3, this suggested a prominent role of V2/V3 in disparity response in MT, and minimized the role of V2/V3 in MT motion response. However, an alternative interpretation of the Ponce et al. study is possible. It is possible that both disparity-selective and motion-selective contributions were lost following V2 inactivation, and that remaining motion response was due to V1 contribution. If so, a possible prediction is that loss of V2 inputs to MT, either direct inputs or indirect inputs such as those through V3A, would compromise processes involving integration of motion and disparity necessary for recovering 3D depth or structure from motion information, something that was not tested in the Ponce study.

Also of note is V3A, which is an area considered to be part of the dorsal pathway and which receives heavily from V2, and in particular V2 thick stripes. V3A has a strong role in motion and depth perception (in comparison to depth perception without motion), one which is more prominent than that of MT or medial superior temporal area (MST) (e.g., Huk et al., 2001; Smith and Wall, 2008). Thus, V3A is another possible route by which V2, and the organized motion maps (this report) and disparity

maps (Chen et al., 2008) in V2, can influence MT and the dorsal pathway. It remains to be determined whether motion and disparity are separately contributing to the dorsal pathway or whether a convergent motion/disparity signal is forwarded to MT. In sum, in addition to the well-studied V1→MT motion pathway, the indirect pathway to MT via V2 (and V3) may play a distinct role in motion information processing.

Possible Role of V2 Motion Signals in the Ventral Pathway

We also consider use of motion signals in ventral pathway function. Although thick stripes project predominantly to MT, there are also ample intra-areal connections within V2 that permit channeling of motion information into the ventral pathway. A recent study has shown that motion signals in layer 4B of V1 originate from two types of neurons. MT-projecting V1 cells are mainly spiny stellate cells, while V2 thick-stripe-projecting cells are mostly pyramidal cells, which are likely to mediate slower computations (Nassi and Callaway, 2007). Such slower computation may not be useful for calculating the speed or direction of the object, but may be useful for object identification (e.g., figure-ground segregation). Peterhans and von der Heydt (1993) found that neurons sensitive to coherent-motion-defined lines are more frequently found in thick stripes. Marcar et al. (2000) found that some neurons in V2 detect the orientation of the border between two moving random dot fields (differential motion border) and that the orientation preference to such motion borders is the same as their preference to the orientation of the luminance borders. Using optical imaging, we have also reported the presence of orientation maps in V2 induced by motion-defined borders, congruent to those obtained with luminance-defined borders (Roe et al., 2009). This evidence suggests that V2 may play an important role in a "motion differentiation process," a role central to figure-ground segregation. Such signals may be used by higher ventral pathway areas such as area V4 for motion-defined shape processing (e.g., Handa et al., 2010).

EXPERIMENTAL PROCEDURES

All surgical and experimental procedures conformed to the guidelines of the National Institutes of Health and were approved by the Vanderbilt Animal Care and Use Committee.

Anesthetized Imaging

In anesthetized experiments, monkeys were anesthetized (thiopental sodium, 1–2 mg/kg/hr intravenously [i.v.] and isoflurane, 0.2%–1.5%), paralyzed with vecuronium bromide (0.05 mg/kg/hr i.v.), and artificially ventilated. Anesthetic depth was assessed continuously via implanted wire electroencephalographic electrodes, end-tidal CO_2, oximetry, and heart rate, and by regular testing for response to toe pinch while monitoring heart rate changes. A craniotomy and durotomy were performed to expose visual areas V1 and V2 (near the lunate sulcus at an eccentricity of 1°–4° from the fovea). In monkey M2, two chronic chambers (diameter 22 mm) were implanted in both hemispheres. In monkeys M1 and M3, one chamber was implanted in the left hemispheres. An artificial dura (Chen et al., 2002) was used to protect the cortex and also help with cortical stabilization. Eyes were dilated (atropine sulfate) and fit with contact lenses of appropriate curvature (Danker Laboratories Inc., Sarasota, FL) to focus on a computer screen 57 cm from the eyes. Risley prisms were placed over each eye and eyes were aligned using a rapid retinotopic imaging method (Lu et al., 2009). Alignment was checked before and after each imaging block. The brain was stabilized with agar and images were obtained through a cover glass.

Images of reflectance change (intrinsic hemodynamic signals) corresponding to local cortical activity were acquired with 632 nm illumination (for details, see Roe and Ts'o, 1995; Lu and Roe, 2008). Signal-to-noise ratio was enhanced by trial averaging (20−100 trials per stimulus condition). Frame size was 504 × 504 pixels and represented either 8 mm × 8 mm or 20 mm × 20 mm of cortical area depending on the imaging lens used. Stimuli were presented in blocks. Each block contained sets of stimuli consisting of either eight gratings of different drifting directions (0°, 22.5°, 45°, 67.5°, 90°, 112.5°, 135°, or 147.5°) or eight random dot patterns (drifting in one of eight directions: 0°, 22.5°, 45°, 67.5°, 90°, 112.5°, 135°, or 147.5°) and a blank. All stimuli were presented in a randomly interleaved fashion.

Awake Imaging and Tasks
Two monkeys (M1 and M2) were trained to sit calmly (head fixed by a head post) and perform a simple fixation task. After initial training, a chronic imaging chamber was implanted over the visual areas V1 and V2 (Chen et al., 2002). Optical maps were collected using the Imager 3001 system (Optical Imaging Inc., Germantown, NY) with 632 nm illumination. Screen distance was either 118 cm or 140 cm from the monkey's eyes. The monkeys were trained to fixate on a fixation spot (0.2°) during the stimulus presentation. The visual stimulus was either a full screen or a 5° rectangular patch that covered the visual field of the cortical area being imaged. In all cases, the fixation spot was placed at the center of the screen. Each condition started with the monkey acquiring and maintaining fixation on the fixation spot for 0.5 s. Thus, there was no stimulus in the first 0.5 s of imaging (imaging of the baseline). The stimulus was then presented in the following 3.5 s. During the imaging period (total of 4 s), the optical signal was collected at a frame rate of 4 Hz (four frames per second, 16 frames total). The monkey received a drop of juice for maintaining fixation throughout the imaging period. Typically, each experiment contained 8–10 stimulus conditions; each condition was repeated 80–100 times. Visual stimuli were identical to those used in anesthetized experiments except for the presence of a central fixation dot.

Visual Stimuli
Visual stimuli were created using VSG 2/5 or ViSaGe (Cambridge Research Systems Ltd., Rochester, UK) and presented on a CRT monitor (SONY GDM F500R). The stimulus screen was gamma corrected and positioned 57 cm (for anesthetized imaging), 118 cm (for awake case 1), or 140 cm (for awake case 3) from the eyes. Mean luminance for all stimuli, including the blank stimulus, was kept at 30 cd/m^2.

Full screen drifting sinusoidal gratings were used to obtain basic functional maps including those for ocular dominance, orientation, and color. Spatial and temporal frequencies were optimized for these maps (see Lu and Roe, 2007). To obtain direction maps, two types of stimuli were used: either drifting sinusoidal gratings or moving random dot patterns. Full field sinusoidal gratings (spatial frequency = 1.5 c/degree, temporal frequency 1 Hz) were presented in eight directions (0°, 45°, 90°, 135°, 180°, 225°, 270°, or 315°). Random dot patterns consisted of white dots (0.04°), presented at a density that covered 10% of the monitor area, and drifted at 4°–8°/s (for direction maps) or 1°/s (for axis-of-motion maps). These stimuli were presented in a randomly interleaved fashion in one of eight directions (0°, 45°, 90°, 135°, 180°, 225°, 270°, or 315°).

Data Analysis
Single Condition Maps
For each stimulus condition, we constructed a "single-condition map." The gray value of each pixel in the "single-condition map" represents the percent change of the light reflectance signal after stimulus onset. Specifically, the gray value of each pixel was calculated using the following function: dR/R = (F$_{avg}$ − F$_0$)/F$_0$ in which dR/R represents percent change, F$_0$ is the average raw reflectance value of the first two frames (taken before stimulus onset and thus representative of the baseline activity), and F$_{avg}$ is the average raw reflectance values of frames 5–16 (1–3.5 s after stimulus onset). Single-condition maps obtained in this way represent the percent intrinsic signal change relative to the initial (prestimulus) baseline. These resulting maps were used for calculating difference maps and vector maps.

Difference Maps
Difference maps were calculated by subtracting two single-condition maps. For example, subtracting the vertical stimulus condition map from the horizontal stimulus condition map results in an orientation map (HV map). Unless otherwise specified, difference maps were clipped at two standard deviations on each side of the median pixel values for display. Maps were usually smoothed (Gaussian filter, 5–8 pixel kernel). Low-frequency noise was reduced by convolving the maps with a 150 pixel diameter circular mean filter and subtracting the result from the smoothed maps.

Vector Maps
Vector maps were calculated for stimuli that have an angular feature (e.g., orientation, direction). Single-condition maps were averaged and low-pass filtered (Gaussian filter, 8–15 pixel diameter). Low-frequency noise was removed by convolving this image with an 80–120 pixel diameter mean filter and subtracting the resulting image from the original image. For each pixel, a vector is calculated based on its response to four different orientations or eight directions (vector summation, Bosking et al., 1997). As a result, two maps were obtained: an "angle map" representing the orientation/direction preference at each pixel (angles of the vectors) and a "magnitude map" representing the strength of the orientation/direction selectivity at each pixel (length of the vectors). We also calculated direction vector maps using the vector-maximum method (Kisvárday et al., 2001). However, we didn't find this method better than the vector-summation method. The reason might be that the stimuli we used are random dots while the vector-maximum method is better performed when grating is used (i.e., when there are large bidirectional responses in the map).

Response Profile
Population response profiles were calculated to assess the overall activation of maps in terms of each pixel's preferred orientation. This method was first introduced in Basole et al. (2003). Briefly, the orientation angle map obtained from vector analysis was used as the reference image. To calculate a population response profile for a given difference map (e.g., a motion-axis map), this map was first assigned a threshold at the median pixel value. Pixels that have values higher than this threshold were weighted (pixel value minus threshold) and summed into 20 orientation bins (0°–180°) based on the preferred orientation (from the vector angle map) for each pixel. The response profile obtained in this way indicates if there is a specific orientation-preferring group of pixels activated. If a map has no spatial correlation to the corresponding orientation map, the profile should be flat.

Frame Misalignment Correction
In awake imaging, motion noise is often induced by animal movement, irregular respiration, body position, and so on. The maximum shift is about 50–100 μm (3–6 pixels). We used a postimaging method to calculate the movement and realigned images frame by frame. Detailed alignment method is discussed elsewhere (Roe, 2007).

SUPPLEMENTAL INFORMATION

Supplemental Information for this article includes two figures and can be found with this article online at doi:10.1016/j.neuron.2010.11.020.

REFERENCES

Albright, T.D., Desimone, R., and Gross, C.G. (1984). Columnar organization of directionally selective cells in visual area MT of the macaque. J. Neurophysiol. *51*, 16–31.

Basole, A., White, L.E., and Fitzpatrick, D. (2003). Mapping multiple features in the population response of visual cortex. Nature *423*, 986–990.

Born, R.T. (2000). Center-surround interactions in the middle temporal visual area of the owl monkey. J. Neurophysiol. *84*, 2658–2669.

Bosking, W.H., Zhang, Y., Schofield, B., and Fitzpatrick, D. (1997). Orientation selectivity and the arrangement of horizontal connections in tree shrew striate cortex. J. Neurosci. *17*, 2112–2127.

Chen, L.M., Heider, B., Williams, G.V., Healy, F.L., Ramsden, B.M., and Roe, A.W. (2002). A chamber and artificial dura method for long-term optical imaging in the monkey. J. Neurosci. Methods *113*, 41–49.

Chen, G., Lu, H.D., and Roe, A.W. (2008). A map for horizontal disparity in monkey V2. Neuron *58*, 442–450.

De Valois, R.L., Yund, E.W., and Hepler, N. (1982). The orientation and direction selectivity of cells in macaque visual cortex. Vision Res. *22*, 531–544.

DeAngelis, G.C., and Newsome, W.T. (1999). Organization of disparity-selective neurons in macaque area MT. J. Neurosci. *19*, 1398–1415.

DeYoe, E.A., and Van Essen, D.C. (1985). Segregation of efferent connections and receptive field properties in visual area V2 of the macaque. Nature *317*, 58–61.

Diogo, A.C., Soares, J.G., Koulakov, A., Albright, T.D., and Gattass, R. (2003). Electrophysiological imaging of functional architecture in the cortical middle temporal visual area of Cebus apella monkey. J. Neurosci. *23*, 3881–3898.

Dow, B.M. (1974). Functional classes of cells and their laminar distribution in monkey visual cortex. J. Neurophysiol. *37*, 927–946.

Gegenfurtner, K.R., Kiper, D.C., and Fenstemaker, S.B. (1996). Processing of color, form, and motion in macaque area V2. Vis. Neurosci. *13*, 161–172.

Geisler, W.S. (1999). Motion streaks provide a spatial code for motion direction. Nature *400*, 65–69.

Geisler, W.S., Albrecht, D.G., Crane, A.M., and Stern, L. (2001). Motion direction signals in the primary visual cortex of cat and monkey. Vis. Neurosci. *18*, 501–516.

Gilbert, C.D. (1977). Laminar differences in receptive field properties of cells in cat primary visual cortex. J. Physiol. *268*, 391–421.

Gur, M., Kagan, I., and Snodderly, D.M. (2005). Orientation and direction selectivity of neurons in V1 of alert monkeys: Functional relationships and laminar distributions. Cereb. Cortex *15*, 1207–1221.

Handa, T., Inoue, M., and Mikami, A. (2010). Neuronal activity during discrimination of shapes defined by motion in area V4. Neuroreport *21*, 532–536.

Hawken, M.J., Parker, A.J., and Lund, J.S. (1988). Laminar organization and contrast sensitivity of direction-selective cells in the striate cortex of the Old World monkey. J. Neurosci. *8*, 3541–3548.

Hubel, D.H., and Livingstone, M.S. (1987). Segregation of form, color, and stereopsis in primate area 18. J. Neurosci. *7*, 3378–3415.

Hubel, D.H., and Wiesel, T.N. (1962). Receptive fields, binocular interaction and functional architecture in the cat's visual cortex. J. Physiol. *160*, 106–154.

Hubel, D.H., and Wiesel, T.N. (1968). Receptive fields and functional architecture of monkey striate cortex. J. Physiol. *195*, 215–243.

Huk, A.C., Ress, D., and Heeger, D.J. (2001). Neuronal basis of the motion aftereffect reconsidered. Neuron *32*, 161–172.

Kaskan, P.M., Dillenburger, B.C., Lu, H.D., Roe, A.W., and Kaas, J.H. (2010). Orientation and direction-of-motion response in the middle temporal visual area (MT) of New World owl monkeys as revealed by intrinsic-signal optical imaging. Frontiers in Neuroscience *4*. 10.3389/fnana.2010.00023.

Kisvárday, Z.F., Buzás, P., and Eysel, U.T. (2001). Calculating direction maps from intrinsic signals revealed by optical imaging. Cereb. Cortex *11*, 636–647.

Levitt, J.B., Kiper, D.C., and Movshon, J.A. (1994). Receptive fields and functional architecture of macaque V2. J. Neurophysiol. *71*, 2517–2542.

Lim, H., Wang, Y., Xiao, Y., Hu, M., and Felleman, D.J. (2009). Organization of hue selectivity in macaque V2 thin stripes. J. Neurophysiol. *102*, 2603–2615.

Livingstone, M.S., and Hubel, D.H. (1984). Anatomy and physiology of a color system in the primate visual cortex. J. Neurosci. *4*, 309–356.

Livingstone, M.S., and Hubel, D.H. (1987). Connections between layer 4B of area 17 and the thick cytochrome oxidase stripes of area 18 in the squirrel monkey. J. Neurosci. *7*, 3371–3377.

Lu, H.D., and Roe, A.W. (2007). Optical imaging of contrast response in Macaque monkey V1 and V2. Cereb. Cortex *17*, 2675–2695.

Lu, H.D., and Roe, A.W. (2008). Functional organization of color domains in V1 and V2 of macaque monkey revealed by optical imaging. Cereb. Cortex *18*, 516–533.

Lu, H.D., Chen, G., Ts'o, D.Y., and Roe, A.W. (2009). A rapid topographic mapping and eye alignment method using optical imaging in Macaque visual cortex. Neuroimage *44*, 636–646.

Malonek, D., Tootell, R.B., and Grinvald, A. (1994). Optical imaging reveals the functional architecture of neurons processing shape and motion in owl monkey area MT. Proc. Biol. Sci. *258*, 109–119.

Mante, V., and Carandini, M. (2005). Mapping of stimulus energy in primary visual cortex. J. Neurophysiol. *94*, 788–798.

Marcar, V.L., Raiguel, S.E., Xiao, D., and Orban, G.A. (2000). Processing of kinetically defined boundaries in areas V1 and V2 of the macaque monkey. J. Neurophysiol. *84*, 2786–2798.

Moutoussis, K., and Zeki, S. (2002). Responses of spectrally selective cells in Macaque area V2 to wavelengths and colors. J. Neurophysiol. *87*, 2104–2112.

Movshon, J.A., and Newsome, W.T. (1996). Visual response properties of striate cortical neurons projecting to area MT in macaque monkeys. J. Neurosci. *16*, 7733–7741.

Munk, M.H., Nowak, L.G., Girard, P., Chounlamountri, N., and Bullier, J. (1995). Visual latencies in cytochrome oxidase bands of macaque area V2. Proc. Natl. Acad. Sci. USA *92*, 988–992.

Nassi, J.J., and Callaway, E.M. (2007). Specialized circuits from primary visual cortex to V2 and area MT. Neuron *55*, 799–808.

Ohki, K., Chung, S., Ch'ng, Y.H., Kara, P., and Reid, R.C. (2005). Functional imaging with cellular resolution reveals precise micro-architecture in visual cortex. Nature *433*, 597–603.

Orban, G.A., Kennedy, H., and Bullier, J. (1986). Velocity sensitivity and direction selectivity of neurons in areas V1 and V2 of the monkey: influence of eccentricity. J. Neurophysiol. *56*, 462–480.

Payne, B.R., Berman, N., and Murphy, E.H. (1981). Organization of direction preferences in cat visual cortex. Brain Res. *211*, 445–450.

Peterhans, E., and von der Heydt, R. (1993). Functional organization of area V2 in the alert macaque. Eur. J. Neurosci. *5*, 509–524.

Ponce, C.R., Lomber, S.G., and Born, R.T. (2008). Integrating motion and depth via parallel pathways. Nat. Neurosci. *11*, 216–223.

Ramsden, B.M., Hung, C.P., and Roe, A.W. (2001). Real and illusory contour processing in area V1 of the primate: A cortical balancing act. Cereb. Cortex *11*, 648–665.

Roe, A.W. (2003). Modular complexity of Area V2 in the Macaque monkey. In The Primate Visual System, C. Collins and J. Kaas, eds. (New York, NY: CRC Press), pp. 109–138.

Roe, A.W. (2007). Long-term optical imaging of intrinsic signals in anesthetized and awake monkeys. Appl. Opt. *46*, 1872–1880.

Roe, A.W., and Ts'o, D.Y. (1995). Visual topography in primate V2: Multiple representation across functional stripes. J. Neurosci. *15*, 3689–3715.

Roe, A.W., and Ts'o, D.Y. (1997). The functional architecture of Area V2 in the Macaque monkey. In Cerebral Cortex, Vol. 12: Extrastriate Cortex in Primates, K. Rockland, J.H. Kaas, and A. Peters, eds. (New York: Plenum Press), pp. 295–333.

Roe, A.W., and Ts'o, D.Y. (1999). Specificity of color connectivity between primate V1 and V2. J. Neurophysiol. *82*, 2719–2731.

Roe, A.W., Lu, H.D., and Hung, C.P. (2005). Cortical processing of a brightness illusion. Proc. Natl. Acad. Sci. USA *102*, 3869–3874.

Roe, A.W., Parker, A.J., Born, R.T., and DeAngelis, G.C. (2007). Disparity channels in early vision. J. Neurosci. *27*, 11820–11831.

Roe, A.W., Lu, H.D., and Chen, G. (2009). In Visual System: Functional architecture of Area V2. The Encyclopedia of Neuroscience, *Volume 10*, L. Squire, ed. (Oxford, UK: Elsevier), pp. 331–349.

Schiller, P.H., Finlay, B.L., and Volman, S.F. (1976). Quantitative studies of single-cell properties in monkey striate cortex. I. Spatiotemporal organization of receptive fields. J. Neurophysiol. *39*, 1288–1319.

Schmolesky, M.T., Wang, Y., Hanes, D.P., Thompson, K.G., Leutgeb, S., Schall, J.D., and Leventhal, A.G. (1998). Signal timing across the macaque visual system. J. Neurophysiol. *79*, 3272–3278.

Schroeder, C.E., Mehta, A.D., and Givre, S.J. (1998). A spatiotemporal profile of visual system activation revealed by current source density analysis in the awake macaque. Cereb. Cortex *8*, 575–592.

Shipp, S., and Zeki, S. (1985). Segregation of pathways leading from area V2 to areas V4 and V5 of macaque monkey visual cortex. Nature *315*, 322–325.

Shipp, S., and Zeki, S. (2002). The functional organization of area V2, I: Specialization across stripes and layers. Vis. Neurosci. *19*, 187–210.

Shmuel, A., and Grinvald, A. (1996). Functional organization for direction of motion and its relationship to orientation maps in cat area 18. J. Neurosci. *16*, 6945–6964.

Shmuel, A., Korman, M., Sterkin, A., Harel, M., Ullman, S., Malach, R., and Grinvald, A. (2005). Retinotopic axis specificity and selective clustering of feedback projections from V2 to V1 in the owl monkey. J. Neurosci. *25*, 2117–2131.

Smith, A.T., and Wall, M.B. (2008). Sensitivity of human visual cortical areas to the stereoscopic depth of a moving stimulus. J. Vis. *8*, 1–12, 1–12.

Swindale, N.V., Matsubara, J.A., and Cynader, M.S. (1987). Surface organization of orientation and direction selectivity in cat area 18. J. Neurosci. *7*, 1414–1427.

Tanaka, K. (1996). Representation of Visual Features of Objects in the Inferotemporal Cortex. Neural Netw. *9*, 1459–1475.

Tolias, A.S., Smirnakis, S.M., Augath, M.A., Trinath, T., and Logothetis, N.K. (2001). Motion processing in the macaque: Revisited with functional magnetic resonance imaging. J. Neurosci. *21*, 8594–8601.

Tootell, R.B., and Hamilton, S.L. (1989). Functional anatomy of the second visual area (V2) in the macaque. J. Neurosci. *9*, 2620–2644.

Ts'o, D.Y., Frostig, R.D., Lieke, E.E., and Grinvald, A. (1990). Functional organization of primate visual cortex revealed by high resolution optical imaging. Science *249*, 417–420.

Ts'o, D.Y., Roe, A.W., and Gilbert, C.D. (2001). A hierarchy of the functional organization for color, form and disparity in primate visual area V2. Vision Res. *41*, 1333–1349.

Vanduffel, W., Fize, D., Mandeville, J.B., Nelissen, K., Van Hecke, P., Rosen, B.R., Tootell, R.B., and Orban, G.A. (2001). Visual motion processing investigated using contrast agent-enhanced fMRI in awake behaving monkeys. Neuron *32*, 565–577.

Wang, G., Tanaka, K., and Tanifuji, M. (1996). Optical imaging of functional organization in the monkey inferotemporal cortex. Science *272*, 1665–1668.

Weliky, M., Bosking, W.H., and Fitzpatrick, D. (1996). A systematic map of direction preference in primary visual cortex. Nature *379*, 725–728.

Xiao, Y., Wang, Y., and Felleman, D.J. (2003). A spatially organized representation of colour in macaque cortical area V2. Nature *421*, 535–539.

Xiao, Y., Casti, A., Xiao, J., and Kaplan, E. (2007). Hue maps in primate striate cortex. Neuroimage *35*, 771–786.

Xu, X., Collins, C.E., Kaskan, P.M., Khaytin, I., Kaas, J.H., and Casagrande, V.A. (2004). Optical imaging of visually evoked responses in prosimian primates reveals conserved features of the middle temporal visual area. Proc. Natl. Acad. Sci. USA *101*, 2566–2571.